Synthesis of Cadmium Telluride Quantum Wires and the Similarity of Their Band Gaps to Those of Equidiameter Cadmium Telluride Quantum Dots

Jianwei Sun,† *Lin-Wang Wang,*‡ *and William E. Buhro*[*,†]

†Department of Chemistry and Center for Materials Innovation, Washington University, St. Louis, Missouri 63130-4899. ‡Lawrence Berkeley National Laboratory, 1 Cyclotron Road, Berkeley, CA 94720.

E-mail: buhro@wustl.edu

Abstract: High-quality colloidal CdTe quantum wires having purposefully controlled diameters in the range of 5-11 nm are grown by the solution-liquid-solid (SLS) method, using Bi-nanoparticle catalysts, cadmium octadecylphosphonate and trioctylphosphine telluride as precursors, and a TOPO solvent. The wires adopt the wurtzite structure, and grow along the [002] direction (parallel to the *c* axis). The size dependence of the band gaps in the wires are determined from the absorption spectra, and compared to the experimental results for high-quality CdTe quantum dots. In contrast to the predictions of an effective-mass approximation, particle-in-a-box model, and previous experimental results from CdSe and InP dot-wire comparisons, the band gaps of CdTe dots and wires of like diameter are found to be experimentally indistinguishable. The present results are analyzed using density functional theory under the local-density approximation by implementing a charge-patching method. The higher-level theoretical analysis finds the general existence of a threshold diameter, above which dot and wire band gaps converge. The origin and magnitude of this threshold diameter is discussed.

Introduction

We report a detailed comparison of the size dependence of the band gaps in colloidal CdTe quantum wires and quantum dots. Interestingly, we find the band gaps of CdTe quantum wires to be experimentally indistinguishable from those of CdTe quantum dots having the same diameters, over the diameter range of our study. A theoretical analysis provides new insights into the comparative electronic properties of quantum dots and wires.

Over the past two decades, semiconductor quantum nanostructures such as quantum dots, rods, wires, and wells have drawn increasing scientific and technological interest.[1-7] Theoretical[8-10] and experimental[11-16] studies have begun to elucidate how the geometric dimensionality of confinement influences the electronic structures of quantum-confined systems. The increasing availability of semiconductor quantum wires has allowed us to draw experimental comparisons between wires and corresponding sets of quantum dots,[13-15] rods,[14,16] and wells.[17]

We have previously compared the confinement in quantum wires and dots using an overly simple effective-mass-approximation, particle-in-box (EMA-PIB) model to estimate the kinetic confinement energies of electron-hole pairs. According to this model, plots of ΔE_g, the increase in the band gap over the bulk value, vs. d^{-2}, the inverse-square diameter, should yield straight lines having slopes that depend on the confinement dimensionality and thus shape of the quantum nanostructure. The slope ratio for dots and wires of the same composition is predicted by the EMA-PIB model to be A_{wire}:A_{dot} = 0.585, and the measured experimental values for InP (A_{wire}:A_{dot} = 0.62 ± 0.03 and 0.66 ± 0.03)[13,15] and CdSe (A_{wire}:A_{dot} = 0.53 ± 0.05)[14] were close to this value. These prior results have confirmed that confinement in the wires is weakened to the expected extent relative to that in dots by the loss of one confinement dimension.

We report here that the A_{wire}:A_{dot} slope ratio extracted from the ΔE_g-vs.-d^{-2} plots for CdTe wires and dots was 1.09, near unity, indicating a convergence of the dot and wire band gaps, over the diameter regime studied. The result stands in contrast to the EMA-PIB prediction, and the wire-dot comparisons

from the CdSe and InP systems. To investigate this disparity, a higher-level theoretical analysis was conducted using the results of density-functional-theory calculations.[10]

The theoretical analysis provided here found that the ΔE_g-vs.-d^{-2} plots for semiconductor wires and dots generally consist of two regimes: a convergence regime *above* a threshold diameter (d_{th}) in which dot and wire band gaps are effectively indistinguishable, and a divergence regime *below* d_{th} in which the A_{wire}:A_{dot} slope ratios approximate the EMA-PIB value of 0.6. The dot-wire comparisons for the CdTe system presented here were thus made in the convergence regime.

The origin and magnitude of the threshold diameter d_{th} is a major emphasis of this report. We propose that the convergence regime results from differing electron-hole Coulomb energies in dots and wires, and that d_{th} increases with decreasing electron-hole Coulomb energy. Thus, as should be expected, the dot-wire systems having comparatively small Coulomb energies conform most closely to the EMA-PIB model.

Experimental Section

Chemicals. Cadmium oxide (CdO, 99.99+%), tellurium (Te, -5+50 mesh, 99.99%), palmitic acid (PA, 99%), trioctylphosphine (TOP, tech., 90%), trioctylphosphine oxide (TOPO, tech., 90%), 2-propanol (99.5%, HPLC grade), and toluene (99.8%, HPLC grade) were purchased from Aldrich and used as received except for TOPO, which was vacuum distilled (~10^{-3} torr) before use. *n*-Octadecylphosphonic acid (ODPA) was purchased from PolyCarbon Industries and used as received.

Preparation of Bi nanoparticles. Bi catalyst nanoparticles were prepared by a modified literature method[14] and detailed syntheses of nanoparticles over a range of sizes will be reported elsewhere.

Preparation of a stock TOPTe solution. The precursor tri-*n*-octylphosphine telluride (TOPTe) was prepared from a mixture of elemental Te (0.256 g, 2 mmol) and TOP (79.744 g). The mixture was stirred at about 240 °C under dry, O_2-free N_2(g) until all elemental Te disappeared (~15 min) to form a transparent yellowish solution. The resulting solution was cooled to room temperature and stored in the

glovebox for use.

General preparation of CdTe nanowires. All procedures were conducted under dry, O_2-free N_2(g). The quantities of reagents used are recorded in Table S1 (Supporting Information). In a typical preparation, CdO, ODPA, and TOPO were loaded into a Schlenk reaction tube. In a separate vial, the Bi-nanoparticle stock solution and TOPTe stock solution were mixed, and the vial was septum capped. The reaction tube was then inserted into a preheated salt bath ($NaNO_3$/KNO_3, 46:54 by weight) at 300-330 °C to obtain a clear solution, and then transferred to another preheated salt bath at a desired temperature (see Table S1). The reaction mixture was allowed equilibrate to the salt bath temperature for several minutes, and then the contents of the vial were quickly injected into the reaction tube by a syringe. Within 10 s the color of the reaction mixture was observed to change to an apparent black (actually a dark red-brown) as the nanowires grew. The reaction tube was withdrawn from the salt bath 5 min after the injection and allowed to cool. Before the reaction mixture was solidified, toluene (~ 5 mL) was added to the reaction tube to prevent solidification. The CdTe-nanowire product was indefinitely stable in this form, and was typically stored in this form.

The CdTe nanowires were separated from the reaction mixture by adding a minimum amount of 2-propanol (~ 5 mL) to the mixture, whereupon the TOPO and soluble byproducts dissolved and the nanowires precipitated. The precipitated wires were collected by centrifugation. The precipitated wires could be redispersed in toluene, hexanes, and chloroform.

Sample Characterization. The UV-Vis absorption spectra of CdTe quantum wires were collected at room temperature using a Varian Cary 100 Bio UV-visible spectrophotometer. Carbon-coated Cu TEM grids were prepared by evaporating one drop of the nanowire toluene solutions on them. Low-resolution TEM images and energy-dispersive X-ray spectroscopy (EDS) were collected using a JEOL 2000 FX microscope operating at 200 kV. High-resolution TEM (HRTEM) images were collected using a JEOL JEM-2100F microscopy operating at 200 kV. The XRD pattern was obtained using a Rigaku Dmax A vertical powder diffractometer with Cu Kα radiation (λ = 1.5418 Å).

Nonlinear least-squares fitting of the UV-Vis absorption spectra. The UV-Vis absorption spectra were fit using a modification of a method reported previously.[13,14] Briefly, each absorption spectrum was converted from a wavelength to an energy scale, and then fit with one exponential (for the background) and multiple Gaussian functions (for the features) using Origin 7.5 software (www.OriginLab.com). The number of Gaussian functions used was determined by the number of absorption features present in the spectra. The fitting procedure yielded the center energy of the excitonic peaks and the error in the center energy (Figure S1, Supporting Information). The quantum-wire band gaps were assigned to the centers of the lowest-energy Gaussian peaks.

Results

Synthesis. For synthesis of CdTe quantum wires, we investigated the use of precursors and conditions previously shown to be successful for the synthesis of high-quality CdTe quantum dots, rods, and tetrapods.[18-21] The cadmium precursors were either cadmium oleate or cadmium octadecylphosphonate generated *in situ* from CdO and oleic acid (OA) or octadecylphosphonic acid (ODPA), respectively.[19] Tri-*n*-octylphosphine telluride (TOPTe) was used as the tellurium precursor. We employed Bi nanoparticles as the catalysts for the growth of CdTe quantum wires, because of their general applicability for the SLS synthesis of various II-VI, III-V, and IV-VI semiconductor nanowires,[14,15,22-28] including CdTe nanowires.[23] To achieve the best control over the wire growth, synthetic conditions including the solvent, cadmium precursor, precursor ratio, and precursor concentration were carefully optimized.

Most of the optimization experiments were conducted using the oleate precursor $Cd(OA)_2$; however, we ultimately determined that the octadecylphosphonate precursor Cd(ODPA) was superior, as is described later. Good success was achieved using a conventional solvent, tri-*n*-octylphosphine oxide (TOPO), although the results depended on the source and batch of TOPO. Reproducible, good results were obtained from 90%-purity, technical-grade TOPO that was vacuum distilled before use.

The Cd:Te precursor ratio (R) strongly influenced the product morphologies. Long, straight wires were obtained when the cadmium precursor was used in excess (R = 3-9). Significantly, catalyst nanoparticles were observed at wire ends (Figures 1 and 2), confirming the SLS growth mechanism.

The concentration of the tellurium precursor TOPTe was also found to be an important synthetic parameter, which influenced the proportions of wires and dots formed. Low concentrations of TOPTe minimized dot formation. The optimal concentration was found to be 0.02 mmol TOPTe per 4 g TOPO.

Although CdTe quantum wires of various mean diameters were successfully prepared using $Cd(OA)_2$ as the cadmium precursor, the formation of quantum dots in small amounts could not be avoided. The dots were presumably formed by homogenous nucleation in a process competing with SLS growth. Peng and coworkers have previously demonstrated that cadmium alkylphosphonate precursors are much less reactive than cadmium carboxylates.[20] Indeed, we found that the use of Cd(ODPA) dramatically suppressed homogeneous nucleation and dot formation under optimized experimental conditions.

The reaction conditions optimized for the $Cd(OA)_2$ precursor were employed with the cadmium alkylphosphonate precursor, which was generally Cd(ODPA). However, in a few cases cadmium *n*-tetradecylphosphonate [Cd(TDPA)] was used with similar success.

Representative low- and high-magnification TEM images of CdTe quantum wires synthesized from Cd(ODPA) (Figures 1 and 2) show that dot formation was nearly eliminated, as indicated by the clean image backgrounds. The diameters of the wires were purposely varied within the range of 5-11 nm. The standard deviation in the diameter distributions was less than 20% of the mean wire diameters (Figure S2). TEM images obtained at the lowest magnification (Figure 1a) established that the wires were typically several micrometers long, and tended to form large bundles having widths up to the micrometer scale. The separations between the individual wires in the bundles were very uniform, and presumably corresponded to the volume occupied by the surfactant coatings on the wire surfaces. The high-magnification images (Figure 2) showed that the nanowires possessed near-constant diameters

along their lengths. The high-resolution TEM (HRTEM) image (Figure 2h) from a wire bundle indicated that the wires were single crystalline over large domains, and crystallographically oriented.

[Insert Figure 1 and 2]

Diameter control was achieved by varying the diameters of the Bi catalyst nanoparticles. Although the size of the catalyst nanoparticles was the most important factor for controlling wire diameters, the reaction temperature was also adjusted in conjunction with variations in catalyst nanoparticle size (Table S1). These temperature variations optimized the wire-diameter control in response to the different melting points and agglomeration tendencies of the variously sized Bi nanoparticles.[29] Thus, a relatively low reaction temperature was used with small Bi nanoparticles, because they have low melting points and a high tendency to agglomerate. However, relatively high reaction temperatures were optimal for larger Bi nanoparticles because of their comparatively higher melting points (and lower agglomeration tendencies).

The diameters of the CdTe quantum wires (d_{CdTe}) were found to scale linearly with the initial diameters of the Bi nanoparticles (d_{Bi}), revealing the relationship in eq. 1 (see Figure S3). The slope value of 0.54 is comparable to the slope values measured in other II-VI and III-V semiconductor-nanowire syntheses by SLS growth.[30] Equation 1 applies only to Bi nanoparticles having diameters within the range of ~5-17 nm. The growth of high-quality CdTe quantum wires having mean diameters of less than 5 nm has not yet been achieved because of the rapid, uncontrolled agglomeration of very small Bi nanoparticles. Very large Bi nanoparticles were also problematic. For example, CdTe wires having a 17.3-nm mean diameter were produced using 40-nm Bi nanoparticles, but the standard deviation in the diameter distributions was measured to be 43.4% of the mean diameter, indicating that the diameter control was very poor.

$$d_{CdTe} = (0.54 \pm 0.06)d_{Bi} + (1.92 \pm 0.68) \quad (1)$$

Structure. The crystal structure of the CdTe quantum wires was investigated by powder X-ray diffraction (XRD, Figure S4) and HRTEM (Figure S5). By comparing the experimental XRD patterns

of the wires with the standard patterns of bulk CdTe having wurtzite and zinc blende structures, the wurtzite structure of the CdTe quantum wires was confirmed. The fast-Fourier-transform (FFT) pattern obtained from the well-resolved HRTEM lattice image was also indexed to the wurtzite structure (inset, Figure S5), indicating the [002] growth direction for the wires (parallel to the *c* axis in the crystal structure). The well-resolved lattice fringes perpendicular to the growth direction corresponded to a spacing of 0.38 nm, consistent with the *d*-spacing between (002) planes in hexagonal CdTe.[31]

[Insert Figure 3]

Figure 3 shows a lattice-resolved HRTEM image of a single CdTe nanowire having a catalyst nanoparticle attached to the wire tip. The catalyst nanoparticle appears darker in the image because of *Z* contrast: $Z_{Bi} > Z_{Te} \approx Z_{Cd}$. Energy-dispersive X-ray spectra (EDS) collected from other wires with attached catalyst nanoparticles (Figure S6) contained only Cd and Te signals from the wires, and only Bi signals from the catalyst nanoparticles. Well-resolved lattice fringes in the Bi nanoparticle tip are evident in the Figure-3 HRTEM image, indicating a recrystallization of Bi upon cooling after the synthesis procedure. Interestingly, the Bi fringe pattern is aligned parallel to the corresponding lattice fringes in the attached CdTe wire, suggesting an epitaxial relationship. The measured lattice spacing in the Bi nanoparticle is 0.398 nm, which matches the 003 *d*-spacing of rhombohedral Bi.[32] Thus, the results indicate an epitaxial junction between Bi (003) and CdTe (002) crystal faces, which is reasonable due to the very small lattice mismatch of 0.5% (Table S2 and Figure S7).

UV-Vis absorption spectra, and the size dependence of the band gap in CdTe quantum wires. The spectroscopic studies and band-gap determinations were conducted with CdTe quantum wires synthesized from Cd(ODPA). Room-temperature UV-Vis absorption spectra collected from the toluene dilutions of the wires contained at least four resolved excitonic features (Figure 4a), consistent with the high quality of the wires. Size-dependent blue shifts of the absorption edges relative to the *bulk* band-edge absorption at 1.50 eV were clearly evident. These blue shifts are quantified as the ΔE_g values referred to below. The lowest-energy feature in each spectrum (Figure 4b) was extracted by empirical

nonlinear least-squares fitting. The band-gap energy for wires of each diameter studied was assigned as the center (Table S1) of the resulting Gaussian-fitted peak.

[Insert Figure 4]

Confinement energies are also often measured from the corresponding peaks in photoluminescence spectra.[33,34] However, we observed only weak room-temperature photoluminescence from the smaller-diameter wires. The photoluminescence from the larger-diameter wires was so weak and noisy that the positions of the peaks could not be accurately determined. We note that the photoluminescence from colloidal semiconductor quantum wires is typically very weak.[15] Consequently, quantum-confinement studies on wires often rely on absorption data.

As noted in the introduction, we have previously compared the confinement in corresponding sets of quantum wires and dots using an effective-mass-approximation, particle-in-box (EMA-PIB) model. This model predicts straight-line plots of ΔE_g vs. d^{-2} (inverse-square diameter) for dots and wires, with a slope ratio of A_{wire}:A_{dot} = 0.585. The measured experimental values for InP (A_{wire}:A_{dot} = 0.62 ± 0.03 and 0.66 ± 0.03)[13,15] and CdSe (A_{wire}:A_{dot} = 0.53 ± 0.05)[14] were consistent with this prediction.

We have similarly compared the confinement in CdTe quantum wires and dots by graphing ΔE_g vs. d^{-2} using the data from Figure 4 and Table S1 for CdTe wires, and data extracted from a publication by Peng and coworkers for CdTe dots (see Figure 5).[20] Linear fits to the wire and dot data yielded the slopes A_{wire} = 7.2 ± 0.3 eV nm^2 and A_{dot} = 6.6 ± 0.3 eV nm^2, respectively. The experimental slope ratio was thus found to be A_{wire}:A_{dot} = 1.09 ± 0.07, which to our initial surprise was far from the theoretical value of 0.585 predicted by the EMA-PIB model.[9,10,13-15] Indeed, the experimental slope ratio near unity indicated that the size dependences of the band gaps in CdTe wires and dots were essentially indistinguishable, over the diameter regime investigated.

[Insert Figure 5]

As noted above and previously,[9,10,13-15] the EMA-PIB model is an overly simple approximation, and the linear fits described above do not fully correspond to the expected confinement behavior. For

example, both the dot and wire lines should extrapolate through the Figure-5 origin, as quantum confinement disappears at large diameters. The EMA-PIB model assumes parabolic band shapes, bulk (size-independent) effective masses, and infinite potential barriers at the dot and wire surfaces, which are severe approximations. Additionally, the model ignores the Coulomb interaction within electron-hole pairs. We will argue later that these Coulomb interactions are important for determining the relative confinement behaviors of dots and wires.

We thus sought to interpret the experimental results in Figure 5 with the assistance of a higher-level theoretical analysis. Li and Wang have recently calculated the size dependence of the band gaps in a series of quantum dots and wires using density functional theory under the local-density approximation by implementing a charge-patching method (DFT-LDA-CPM) and with LDA band-gap corrections.[10] By this method, the band gaps of dots and wires were calculated over a range of specific diameters, and the results were fit with eq. 2, where α and β are fitting parameters that were found to depend on both nanostructure composition and shape. For CdTe quantum dots and wires, the fitting parameters were $\alpha_{dot} = 1.69$, $\beta_{dot} = 4.38$, $\alpha_{wire} = 1.24$, and $\beta_{wire} = 2.05$. The resulting fitted curves are plotted in Figure 5 (as dashed curves).

$$\Delta E_g = \beta d^{-\alpha} \qquad (2)$$

Several aspects of the DFT-LDA-CPM curves in Figure 5 merit consideration. First, these curves lie below the experimental data for CdTe dots and wires, indicating that the theoretical results have underestimated the experimental confinement energies. However, the theoretical curves were extrapolated from calculations on ranges of specific diameters that were smaller than the diameter ranges employed in the experimental studies. Thus, if additional calculations were completed for larger diameters contained within the experimental diameter ranges, the absolute agreement between the theoretical and experimental data should improve, as was previously found for InP quantum wires.[15] Therefore, the curves plotted in Figure 5 will be useful here for relative rather than absolute comparisons to the experimental data.

More interestingly, the α values (α_{dot} = 1.69, α_{wire} = 1.24) from the DFT-LDA-CPM results differ from the value of 2 determined by the simplistic EMA-PIB model. At higher levels of theory the dot and wire band gaps do not scale with d^{-2}, but rather with $d^{-\alpha}$ where α is in the range of 1-2.[10] These differences are obviously responsible for the gentle curvature of the theoretical plots in Figure 5. As a result of the curvature, the theoretical fits *do* extrapolate through the Figure-5 origin, as they should. Note also that the differences in the α and β values for dots and wires cause the theoretical curves to cross one another. We will refer to this crossover point as the threshold diameter, d_{th}, which for CdTe dots and wires is found to be 5.40 nm.

We do not believe that the curve crossing in Figure 5 is physically real, as 2D-confinement in wires should not exceed the 3D-confinement in the corresponding dots.[9,10] Rather, the curve crossing is likely an artifact of the curve extrapolations from the band-gap calculations for smaller diameter dots and wires (see above). Consequently, here we interpret the crossover point as the threshold diameter (d_{th}), *above* which the dot and wire curves approach one another closely (see Figure 5). That is, we will use d_{th} as the minimum approximate diameter at which the dot and wire curves effectively converge. As a consequence of this effective convergence, for diameters *greater* than d_{th}, the dot and wire band gaps become, in practice, experimentally indistinguishable.

The experimental comparisons of CdTe dot and wire band gaps in Figure 5 were limited to the diameter range of 5-10 nm, because we are presently unable to synthesize CdTe quantum wires having diameters < 5 nm. As this diameter range lies *above* the theoretical d_{th} for CdTe dots and wires, we were limited to comparisons in the convergence regime where dot and wire band gaps are indistinguishable. Consequently, we measured an experimental slope ratio within this size regime of A_{wire}:A_{dot} = 1.09 (see above), near unity, in accord with the higher-level theoretical predictions.

Interestingly, we applied linear fits to the theoretical curves in Figure 5 in the *other* regime, in which the diameters were less than d_{th}, and in which the dot and wire curves *diverge*. We then calculated a "theoretical" slope ratio of A_{wire}:A_{dot} = 0.63 ± 0.01 for this small-diameter, divergence regime. The

value calculated is close to the slope ratio of 0.585 predicted by the simple EMA-PIB model. The result suggests that if we are ultimately able to collect band-gap data from smaller-diameter CdTe wires, a slope ratio close to the EMA-PIB prediction may yet be observed, within the divergence regime. Consequently, two regimes apparently exist in band-gap comparisons of CdTe dots and wires, for diameters *above* and *below* d_{th}. In the large-diameter regime the band gaps converge and are thus indistinguishable, leading to a slope ratio near unity. In the small-diameter regime the band gaps diverge and the dot-wire slope ratios should be close to 0.6, in accord with our prior EMA-PIB rule of thumb.[13-15]

Therefore, we may anticipate this two-regime, divergence-convergence behavior to be general. A threshold diameter, d_{th}, may exist in other similar comparisons of semiconductor dots and wires, above which dot and wire band gaps are effectively indistinguishable. Our previous comparisons of InP[13,15] and CdSe[14] dots and wires found slope ratios near 0.6, suggesting that they were made in the divergence regimes and thus the d_{th} values are comparatively large in those cases. In the CdTe case reported here, the d_{th} value is shown theoretically and experimentally to be smaller. An obvious question arises. What determines whether d_{th} will be relatively large or small? In the following discussion the physical origin of and factors influencing the value of d_{th} are explored.

Discussion

We first address how the theoretical threshold diameter d_{th} for semiconductor dots and wires may be extracted from the relevant DFT-LDA-CPM data. Table 1 records the α and β values of quantum dots and wires for several II-VI and III-V compositions. These values were obtained directly from Li and Wang,[10] or by fitting their theoretical band-gap data. The value of d_{th} was determined by setting wire and dot band gaps equal at d_{th} (eq. 3), and solving for d_{th} (eq. 4). The d_{th} values calculated from eq. 4 are also recorded in Table 1. They range from 0.07 nm for AlN to 2859 nm for GaAs.

[Insert Table 1]

$$\beta_{\text{dot}} d_{\text{th}}^{-\alpha_{\text{dot}}} = \beta_{\text{wire}} d_{\text{th}}^{-\alpha_{\text{wire}}} \quad (3)$$

$$d_{\text{th}} = (\beta_{\text{dot}} / \beta_{\text{wire}})^{1/(\alpha_{\text{dot}} - \alpha_{\text{wire}})} \quad (4)$$

Equation 4 establishes that d_{th} depends on two new, combined parameters, (α_{dot}-α_{wire}) and $\beta_{\text{dot}}/\beta_{\text{wire}}$. The dependence of d_{th} on these combined parameters is plotted in Figure S8. If (α_{dot}-α_{wire}) is small (≤ 0.10) and positive, then $\beta_{\text{dot}}/\beta_{\text{wire}} \geq 1.3$ is sufficient to produce a large d_{th} (≥ 10 nm). As (α_{dot}-α_{wire}) becomes larger, then larger $\beta_{\text{dot}}/\beta_{\text{wire}}$ values are required to produce a large d_{th}. In two cases (Table 1), negative values of (α_{dot}-α_{wire}) are found, indicating that at diameters less than d_{th} the confinement in wires is stronger than that in dots, which is initially counterintuitive. For one such case, CdSe, we will argue below that the negative (α_{dot}-α_{wire}) value is likely to be incorrect. Although we have catalogued here the relative values of (α_{dot}-α_{wire}) and $\beta_{\text{dot}}/\beta_{\text{wire}}$ necessary to produce a large d_{th}, the physical origin of these dependences remains to be elucidated.

The simple EMA-PIB model referred to above, which accounts only for the kinetic confinement energies of electrons and holes and ignores the Coulomb energies associated with their interactions, predicts that dot and wire band gaps should converge only at infinite d, which in practice would be at 2-3 times the bulk exciton Bohr radius. According to Table 1, the DFT-LDA-CPM calculations indicate that convergence may occur at smaller d_{th} values, but what physical effect(s) should drive such convergence? We note here that the LDA-CPM calculations for dots may either include or omit the Coulomb energies resulting from interactions of electrons and holes, and the data in Table 1 are obtained from dot calculations that have *included* the Coulomb contributions. In contrast, an ab initio theoretical method for estimating the Coulomb interactions in wires has not yet to our knowledge been developed.[35-37] Thus the Coulomb contributions, which are presumed to be smaller in wires than in dots,[8,38-40] are *not included* in the Table-1 data for wires. We next consider that such Coulomb interactions in dots and wires may be responsible, at least in part, for their band-gap convergence at relatively small diameters.

One means of assessing the influence of electron-hole Coulomb energies on dot-wire band-gap convergence is to compare calculated d_{th} values when the Coulomb interactions in the dots have been included and omitted, respectively. Ideally the comparison here would use theoretical data for CdTe dots and wires. However, band-gap data for CdTe quantum dots with omission of the Coulomb interactions were not reported.[10] Consequently, we make the comparison using theoretical data for the closely related ZnTe dots and wires.

Figure 6 plots the theoretical diameter dependence of the band gaps in ZnTe wires, ZnTe dots *without* Coulomb interactions, and ZnTe dots *with* Coulomb interactions, using the data from Li and Wang.[10] As expected, the Coulomb interactions *decrease* the band gaps in the dots, such that the curve for dots with Coulomb interactions lies below the curve for dots without them. A consequence of this curve lowering is an apparent decrease in d_{th}; that is, the crossing point of the dot and wire curves moves to a smaller diameter. The d_{th} calculated from eq. 4 with the dot curve omitting Coulomb interactions is 72.1 nm. (This finite d_{th} value is likely an artifact of fitting the theoretical results to the eq. 2 approximation; the value probably should be infinite because the kinetic confinement energy in a dot should always be larger than that in a wire of equal diameter.) This d_{th} value shrinks to 15.4 nm when the dot curve including Coulomb interactions is used. Therefore, strong Coulomb interactions in the dots relative to the wires will generally enforce a smaller d_{th}.

[Insert Figure 6]

The comparison above suggests a rationale for the relative magnitude of d_{th}. For compositions in which the Coulomb interactions are relatively small, they should be small in *both* dots and wires. Consequently, relatively large d_{th} values should obtain, and the A_{wire}:A_{dot} slope ratios (as defined herein) over limited diameter ranges *below* d_{th} should approach the rule-of-thumb value of 0.6 predicted by the EMA-PIB model. In contrast, for compositions in which the Coulomb interactions are relatively large, they should be *larger* in dots than in the corresponding wires, under the above assumption that the electron-hole Coulomb energies are generally smaller in wires due to the relaxation of the third

confinement dimension.[8,38-40] Consequently, in these cases the d_{th} values should be comparatively smaller and convergence of dot and wire band gaps thus achieved at smaller threshold diameters.

Therefore, we now look for an empirical correlation between the calculated d_{th} values in Table 1 and the Coulomb energies in various semiconductors. We represent the Coulomb energies with calculated bulk exciton binding energies ($E_{b,ex}$), which in turn depend on electron and hole effective masses in and the bulk dielectric constants of semiconductors. These values are also reported in Table 1. Figure 7 is a log-normal plot of d_{th} vs. $E_{b,ex}$, in which an empirical correlation is clearly evident. In general, the smaller bulk exciton binding energies correspond to the larger threshold diameters, and visa versa. (Note that the d_{th} values in Figure 7 were obtained from eq. 4 using α and β values from the dot calculations that *included* Coulomb interactions.)

[Insert Figure 7]

The green dashed line drawn in Figure 7 at a threshold diameter of 10 nm estimates our current experimental limitation for characterizing the divergence regime for a set of quantum dots and wires; that is, for measuring an A_{wire}:A_{dot} slope ratio approaching the EMA-PIB rule-of-thumb value of 0.6. We estimate this value of 10 nm by considering that a slope determination would ideally span a wire diameter range of at least 5 nm, and that 5 nm is the approximate lower limit to the diameters of the wires we can presently synthesize. Recall that the EMA-PIB slope ratio should be observed only within diameter ranges below d_{th}. Consequently, for semiconductors having $d_{th} < 10$ nm, we will not have access to a sufficiently wide diameter range for a reliable A_{wire} determination within the divergence regime.

Therefore, for semiconductors below the green line in Figure 7, we should measure experimental A_{wire}:A_{dot} slope ratios approaching unity, for the diameter range we have general access to (5-12 nm). For those above the green line we should measure experimental A_{wire}:A_{dot} slope ratios approaching 0.6. The semiconductor CdTe falls below the line, and we report herein an experimental slope ratio near unity. In contrast, InP falls above the line and we previously reported A_{wire}:A_{dot} slope ratios of 0.62 and

0.66.[13,15] The semiconductor GaAs also falls above the line, and we have measured A_{wire} for this system.[17] Unfortunately, experimental band-gap data for GaAs quantum dots are not available, and so A_{dot} and A_{wire}:A_{dot} are not known. However, the EMA-PIB model predicts a slope ratio for corresponding sets of quantum *wells* and quantum wires of A_{well}:A_{wire} = 0.427, and we determined experimental A_{well}:A_{wire} values of 0.41-0.49.[17] The very large wire-dot d_{th} value (Table 1) for GaAs is a consequence of the very small Coulomb energy, and a similarly large well-wire d_{th} value can be safely assumed. Thus, the results for the CdTe, InP, and GaAs systems are consistent with the analysis proposed here and depicted in Figure 7.

A contradiction to the analysis above is presented by the experimental results for the CdSe system. The position of CdSe in Figure 7, far below the green line, suggests that we should find an experimental A_{wire}:A_{dot} slope ratio near unity, whereas we have measured A_{wire}:A_{dot} to be 0.53,[14] close to the EMA-PIB value. That is, our experimental CdSe dot-wire comparisons are clearly in the divergence regime, whereas Figure 7 predicts they should be in the convergence regime. As previously indicated, CdSe is one of only two cases in Table 1 for which theory finds a negative (α_{dot}-α_{wire}) value. A negative (α_{dot}-α_{wire}) requires that in the divergence diameter regime, the wires will have *larger* band gaps than the dots. Our experimental results show the opposite;[14] CdSe wires exhibit *smaller* band gaps than the dots of like diameter, as is normally expected. We note the possibility of significant errors in the theoretical α and β values reported in Table 1, as a consequence of the fittings and extrapolations used in their determination. Therefore, we believe that eq. 4 should not be used to calculate d_{th} in cases having negative (α_{dot}-α_{wire}) values. Instead, precise non-extrapolated theoretical and/or experimental data should be used. The experimental finding of a normal divergence regime for CdSe dots and wires in the diameter range of 5-11 nm strongly suggests that the d_{th} value for CdSe is indeed > 10 nm, *above* the green line in Figure 7.

We do not argue that the electron-hole Coulomb energy is the only factor influencing the magnitude of the threshold diameter d_{th}. Figure 7 contains considerable scatter, and shows several pair-wise

relationships that are not fully consistent with the Coulomb-energy explanation. For example, the calculated bulk exciton-binding energy in CdTe is smaller than that in InN, but a smaller threshold diameter is determined for CdTe than for InN (Table 1). Analysis of other factors also contributing to d_{th} will require further theoretical study. We also note that the theoretical d_{th} values calculated by eq. 4 contain uncertainties resulting from the use of fitted, extrapolated α and β values. Even so, the empirical relationship between d_{th} and the exciton-binding energy revealed in Figure 7 is strongly suggestive of a significant influence by electron-hole Coulomb energies.

Conclusion

We initiated this study to further test our rule of thumb derived from the EMA-PIB model that plots of ΔE_g vs. d^{-2} for corresponding sets of quantum dots and wires should be approximately linear, and have dot-wire slope ratios close to 0.6.[9,10,13-15] That rule of thumb was found to break down for CdTe dots and wires. The analysis herein reached the conclusion that the EMA-PIB slope ratio should be observed only within a divergence diameter regime below a threshold diameter d_{th}, which decreases with increasing electron-hole Coulomb energy. In retrospect, the conclusion is almost obvious. As the EMA-PIB model does not account for Coulomb energies, it should break down whenever Coulomb energies become significant in comparison to the kinetic confinement energies of electrons (or holes). Our analysis also proposes that in certain cases there is a diameter regime in which *quantum-confined* dot and wire band-gaps converge, producing slope ratios near unity. To date, the CdTe system provides our only known example. However, as there are many semiconductors below the green line in Figure 7, other potential systems exist for testing this proposal, when we are able to synthesize quantum wires having smaller diameters. Observing both the convergence and divergence regimes for a single system should also then be possible.

Acknowledgment. JS and WEB thank Prof. Richard A. Loomis and Dr. John G. Glennon for helpful discussions, and the National Science Foundation (grant no. CHE-0518427) for support. JS is grateful to Tyrone L. Daulton for the high-resolution TEM training. LWW is supported by BES/SC of the U.S. Department of Energy under contract No. DE-AC02-05CH11231. The theoretical calculations used the resources of the National Energy Research Scientific Computing Center (NERSC).

Supporting Information Available: Additional synthetic conditions, spectroscopic data, and supporting results. This material is available free of charge via the Internet at http://pubs.acs.org.

References

(1) Bhattacharya, P. K.; Dutta, N. K. *Annu. Rev. Mater. Sci.* **1993**, *23*, 79-123.

(2) Alivisatos, A. P. *Science* **1996**, *271*, 933-937.

(3) Xia, Y.; Yang, P.; Sun, Y.; Wu, Y.; Mayers, B.; Gates, B.; Yin, Y.; Kim, F.; Yan, H. *Adv. Mater.* **2003**, *15*, 353-389.

(4) Buhro, W. E.; Colvin, V. L. *Nat. Mater.* **2003**, *2*, 138-139.

(5) Law, M.; Goldberger, J.; Yang, P. *Annu. Rev. Mater. Res.* **2004**, *34*, 83-122.

(6) Bhattacharya, P.; Ghosh, S.; Stiff-Roberts, A. D. *Annu. Rev. Mater. Res.* **2004**, *34*, 1-40.

(7) Michalet, X.; Pinaud, F. F.; Bentolila, L. A.; Tsay, J. M.; Doose, S.; Li, J. J.; Sundaresan, G.; Wu, A. M.; Gambhir, S. S.; Weiss, S. *Science* **2005**, *307*, 538-544.

(8) Yoffe, A. D. *Adv. Phys.* **2002**, *51*, 799-890.

(9) Li, J.; Wang, L. W. *Chem. Mater.* **2004**, *16*, 4012-4015.

(10) Li, J.; Wang, L.-W. *Phys. Rev. B* **2005**, *72*, 125325.

(11) Tang, Z.; Kotov, N. A.; Giersig, M. *Science* **2002**, *297*, 237-240.

(12) Kan, S.; Mokari, T.; Rothenberg, E.; Banin, U. *Nat. Mater.* **2003**, *2*, 155-158.

(13) Yu, H.; Li, J.; Loomis, R. A.; Wang, L.-W.; Buhro, W. E. *Nat. Mater.* **2003**, *2*, 517-520.

(14) Yu, H.; Li, J.; Loomis, R. A.; Gibbons, P. C.; Wang, L. W.; Buhro, W. E. *J. Am. Chem. Soc.* **2003**, *125*, 16168-16169.

(15) Wang, F.; Yu, H.; Li, J.; Hang, Q.; Zemlyanov, D.; Gibbons, P. C.; Wang, L. W.; Janes, D. B.; Buhro, W. E. *J. Am. Chem. Soc.* **2007**, *129*, 14327-14335.

(16) Wang, F.; Buhro, W. E. *J. Am. Chem. Soc.* **2007**, *129*, 14381-14387.

(17) Dong, A.; Yu, H.; Wang F.; Buhro, W. E. **Submitted**.

(18) Murray, C. B.; Norris, D. J.; Bawendi, M. G. *J. Am. Chem. Soc.* **1993**, *115*, 8706-15.

(19) Peng, Z. A.; Peng, X. *J. Am. Chem. Soc.* **2001**, *123*, 183-184.

(20) Yu, W. W.; Wang, Y. A.; Peng, X. *Chem. Mater.* **2003**, *15*, 4300-4308.

(21) Manna, L.; Milliron, D. J.; Meisel, A.; Scher, E. C.; Alivisatos, A. P. *Nat. Mater.* **2003**, *2*, 382-385.

(22) Grebinski, J. W.; Hull, K. L.; Zhang, J.; Kosel, T. H.; Kuno, M. *Chem. Mater.* **2004**, *16*, 5260-5272.

(23) Kuno, M.; Ahmad, O.; Protasenko, V.; Bacinello, D.; Kosel, T. H. *Chem. Mater.* **2006**, *18*, 5722-5732.

(24) Dong, A.; Wang, F.; Daulton, T. L.; Buhro, W. E. *Nano Lett.* **2007**, *7*, 1308-1313.

(25) Ouyang, L.; Maher, K. N.; Yu, C. L.; McCarty, J.; Park, H. *J. Am. Chem. Soc.* **2007**, *129*, 133-

138.

(26) Fanfair, D. D.; Korgel, B. A. *Chem. Mater.* **2007**, *19*, 4943-4948.

(27) Fanfair, D. D.; Korgel, B. A. *Cryst. Growth Des.* **2005**, *5*, 1971-1976.

(28) Hull, K. L.; Grebinski, J. W.; Kosel, T. H.; Kuno, M. *Chem. Mater.* **2005**, *17*, 4416-4425.

(29) Olson, E. A.; Efremov, M. Y.; Zhang, M.; Zhang, Z.; Allen, L. H. *J. Appl. Phys.* **2005**, *97*, 034304.

(30) Wang, F.; Dong, A.; Sun, J.; Tang, R.; Yu, H.; Buhro, W. E. *Inorg. Chem.* **2006**, *45*, 7511-7521.

(31) ICDD-PDF No. 01-080-0019.

(32) ICDD-PDF No. 00-044-1246.

(33) Li, L.-S.; Hu, J.; Yang, W.; Alivisatos, A. P. *Nano Lett.* **2001**, *1*, 349-351.

(34) Pietryga, J. M.; Schaller, R. D.; Werder, D.; Stewart, M. H.; Klimov, V. I.; Hollingsworth, J. A. *J. Am. Chem. Soc.* **2004**, *126*, 11752-11753.

(35) Slachmuylders, A. F.; Partoens, B.; Magnus, W.; Peeters, F. M. *Phys. Rev. B* **2006**, *74*, 235321.

(36) Xia, J.-B.; Cheah, K. W. *Phys. Rev. B* **1997**, *55*, 1596-1601.

(37) Bányai, L.; Galbraith, I.; Ell, C.; Haug, H. *Phys. Rev. B* **1987**, *36*, 6099-6104.

(38) Li, J.; Wang, L.-W. *Nano Lett.* **2003**, *3*, 101-105.

(39) Huang, W.; Jain, F. *J. Appl. Phys.* **2000**, *87*, 7354-7359.

(40) Bayer, M.; Walck, S. N.; Reinecke, T. L.; Forchel, A. *Phys. Rev. B* **1998**, *57*, 6584-6591.

Table 1. Bohr radii, α and β parameters, threshold diameters, and calculated bulk exciton-binding energies for various II-VI and III-V systems.

Material[a]	a_B (nm)	Dot		Wire		α_{dot}-α_{wire}	β_{dot}/β_{wire}	d_{th}[b] (nm)	μ[c] (m_e)	ε_{semi}[d]	$E_{b,ex}$[e] (meV)
		α_{dot}	β_{dot}	α_{wire}	β_{wire}						
ZnO (W)	2.3	1.35	0.96	1.85	1.58	-0.50	0.61	2.71	0.19	8.1	38.9
ZnS (W)	2.5	1.28	1.36	1.16	1.24	0.12	1.10	2.16	0.20	9.6	29.5
ZnSe (ZB)	3.8	1.49	2.54	1.29	1.79	0.20	1.42	5.75	0.13	8.6	24.3
ZnTe (ZB)	5.2	1.40	3.00	1.19	1.69	0.21	1.78	15.4	0.10	10.3	13.0
CdS (W)	2.8	1.45	2.08	1.27	1.72	0.18	1.21	2.87	0.16	8.43	30.3
CdSe (W)	5.6	1.18	2.12	1.24	1.95	-0.06	1.09	0.25	0.094	9.57	14.0
CdTe (ZB)	7.5	1.69	4.38	1.24	2.05	0.45	2.14	5.40	0.085	10.4	10.7
AlN (W)	1.9	1.29	0.57	1.12	0.89	0.17	0.64	0.07	0.26	9.14	42.5
GaN (W)	2.8	1.36	1.98	1.15	1.57	0.21	1.26	3.02	0.18	10.1	24.1
GaAs (ZB)	12.5	1.02	2.95	0.96	1.83	0.06	1.61	2859	0.062	12.80	5.1
InN (W)	5.1	1.08	2.29	1.04	1.86	0.04	1.23	181	0.097	9.3	15.2
InP (ZB)	10	1.31	3.36	1.16	2.00	0.15	1.68	31.8	0.069	12.56	5.9
InAs (ZB)	35	1.21	4.11	1.02	2.38	0.19	1.73	17.7	0.025	15.15	1.5

[a]The structure of each material is indicated in parentheses. W and ZB stand for wurtzite and zinc blende, respectively. [b]Calculated from $d_{th} = (\beta_{dot} / \beta_{wire})^{1/(\alpha_{dot}-\alpha_{wire})}$. [c]Reduced exciton mass calculated from $\mu = m_e^* m_h^*/(m_e^* + m_h^*)$. [d]Dielectric constant (ε_{semi}) of the semiconductor material. [e]Exciton binding energy calculated from $E_{b,ex} = \mu e^4(8h^2\varepsilon_{semi}^2\varepsilon_0^2)^{-1}$, according to reference 8. The m_e^*, m_h^*, and ε_{semi} data were taken from: Madelung, O. *Semiconductors: Data Handbook*, 3rd ed.;.Springer: Berlin, 2004, and Madelung, O. *Semiconductors - Basic Data*, 2nd ed.; Springer: Berlin, 1996.

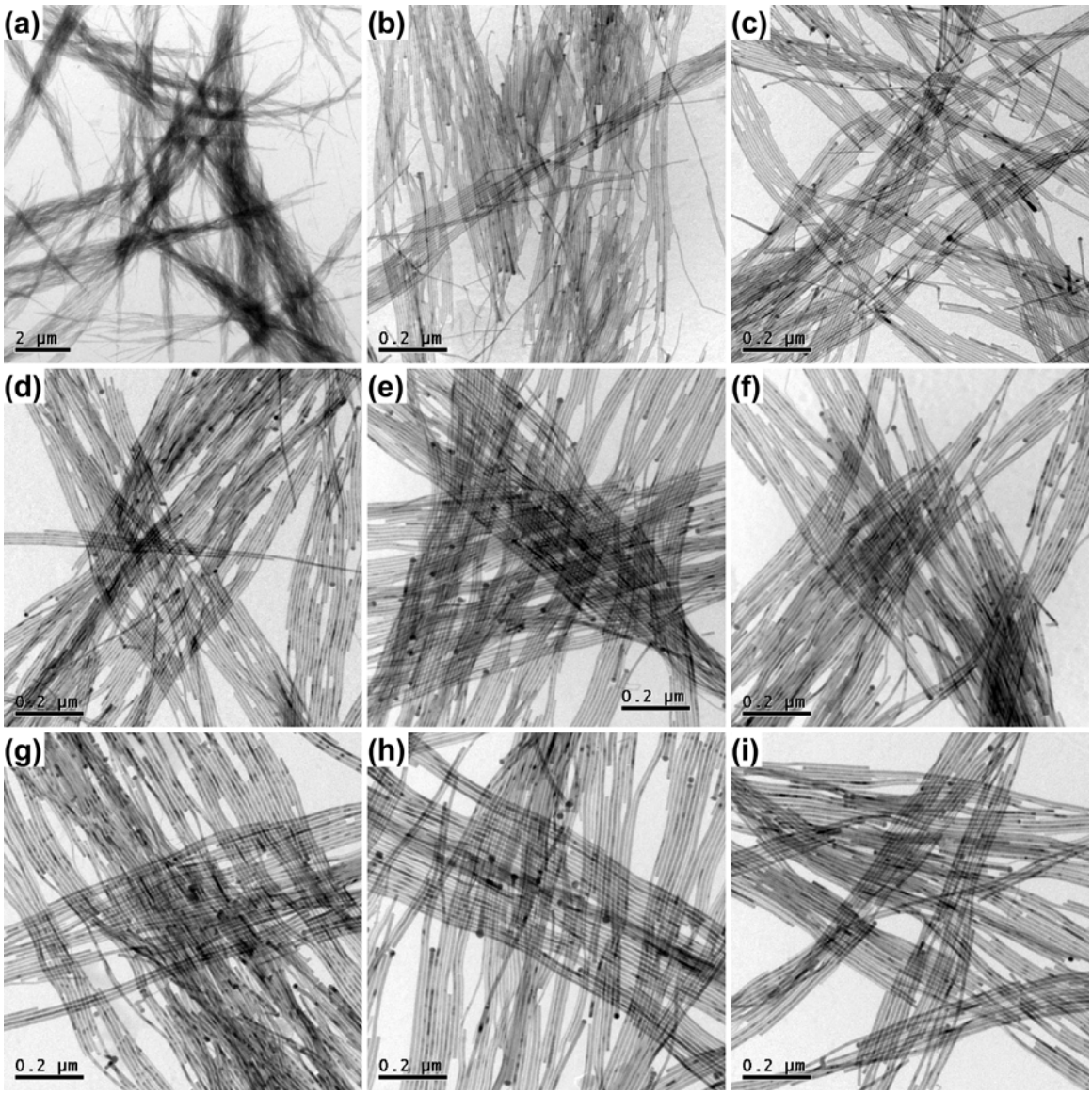

Figure 1. Representative low-magnification TEM images of CdTe quantum wires of various diameters (*d*). (a) $d = 7.3 \pm 1.0$ nm (± 13.7%). This image at low magnification shows that the lengths of the wires are typically several micrometers and that the wires form bundles having widths of up to micrometers. (b) $d = 5.3 \pm 1.1$ nm (± 20.8%), (c) $d = 5.8 \pm 1.0$ nm (± 17.2%), (d) $d = 7.4 \pm 0.9$ nm (± 12.2%), (e) $d = 7.9 \pm 1.3$ nm (± 16.5%), (f) $d = 8.7 \pm 1.5$ nm (± 17.2%), (g) $d = 9.3 \pm 1.6$ nm (± 17.2%), (h) $d = 9.7 \pm 2.0$ nm (± 20.6%), and (i) $d = 10.2 \pm 1.7$ nm (± 16.7%). Individual wires in bundles can be clearly seen in images (b) through (i).

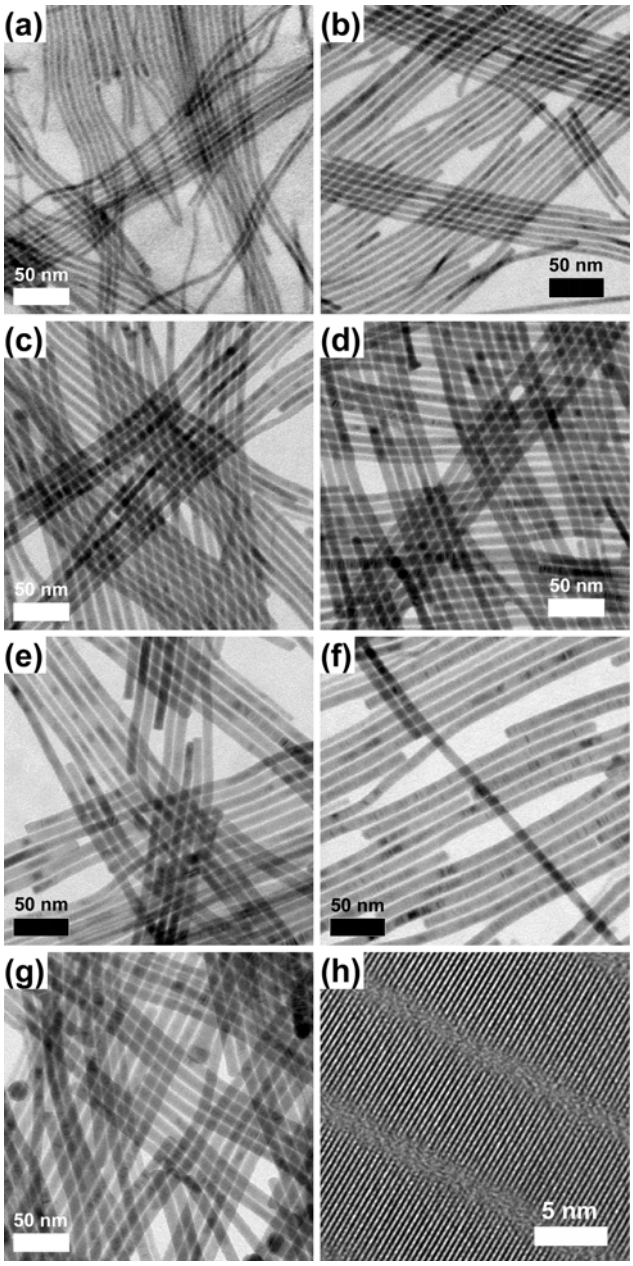

Figure 2. Representative high-magnification TEM images of CdTe quantum wires of various diameters (*d*). (a) $d = 5.3 \pm 1.1$ nm (± 20.8%), (b) $d = 5.8 \pm 1.0$ nm (± 17.2%), (c) $d = 7.3 \pm 1.0$ nm (± 13.7%), (d) $d = 7.9 \pm 1.3$ nm (± 16.5%), (e) $d = 8.7 \pm 1.5$ nm (± 17.2%), (f) $d = 9.3 \pm 1.6$ nm (± 17.2%), and (g) $d = 10.2 \pm 1.7$ nm (± 16.7%). (h) High-resolution TEM (HRTEM) image of CdTe quantum wires with parallel arrangement, indicating that the wires are single crystalline and highly uniform.

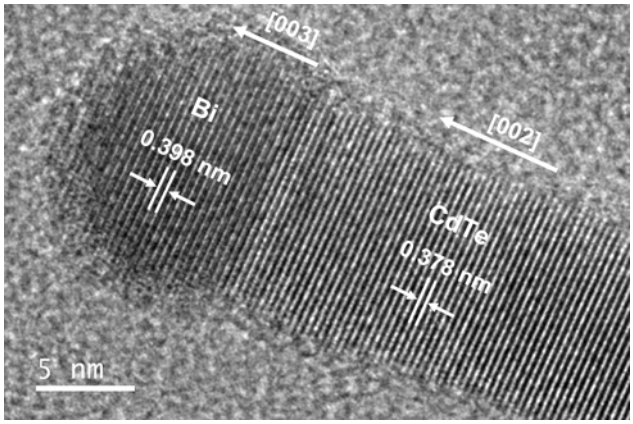

Figure 3. High-resolution TEM image of a single CdTe quantum wire with a catalyst nanoparticle attached to the wire tip.

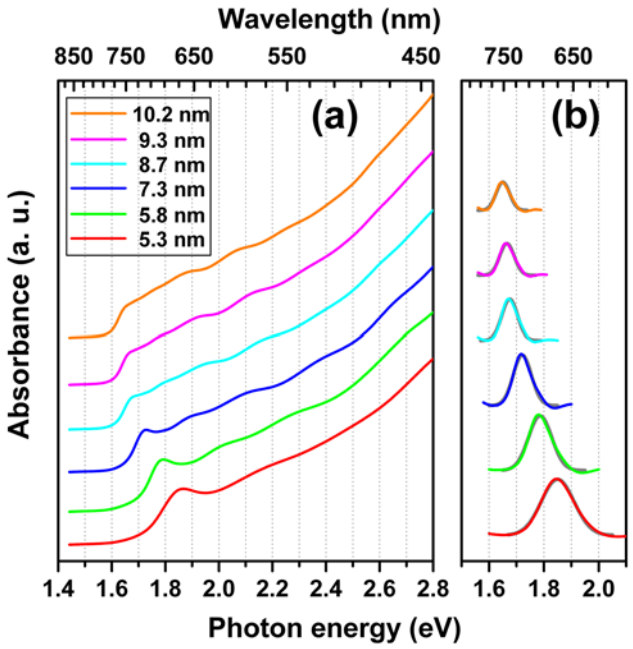

Figure 4. (a) Representative absorption spectra of CdTe quantum wires of various diameters in the range of 5.3-10.2 nm. (b) Lowest-energy excitonic peaks extracted by nonlinear least-squares fitting.

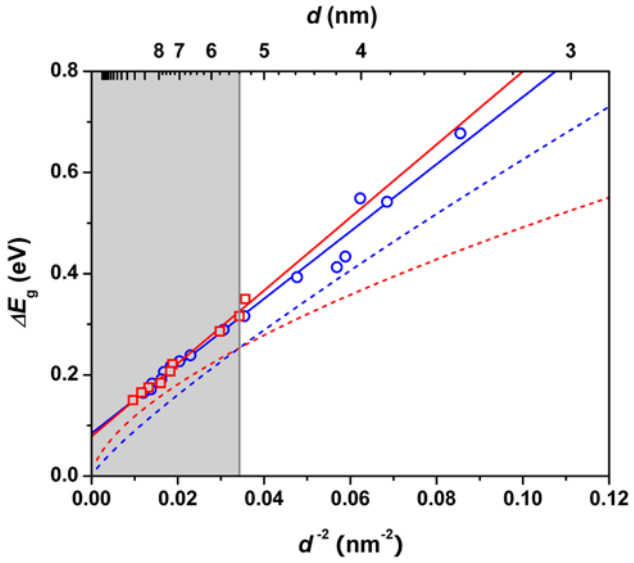

Figure 5. Experimental CdTe quantum-wire data (red open squares) and quantum-dot data (blue open circles) plotted as ΔE_g vs d^{-2}. The dot data were extracted from reference 20. The red and blue solid lines are the linear least-squares fits to the wire and dot data, respectively, yielding the slopes A_{wire} = 7.2 ± 0.3 eV nm^2 and A_{dot} = 6.6 ± 0.3 eV nm^2, and the ratio of the slopes A_{wire}:A_{dot} = 1.09 ± 0.07. Theoretical curves obtained by DFT-LDA-CPM calculations[10] for CdTe quantum wires (red dashed line) and quantum dots (blue dashed line) are also shown.

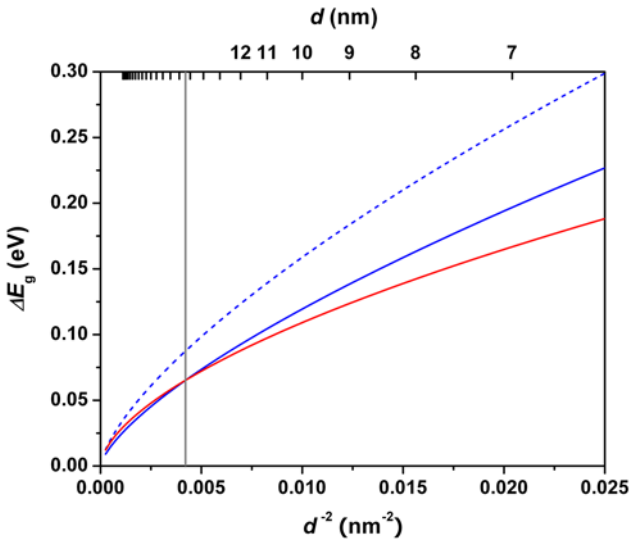

Figure 6. Theoretical ZnTe quantum-wire (red) and quantum-dot (dashed blue, no Coulomb energy; solid blue, including Coulomb energy) curves plotted as ΔE_g vs d^{-2}. These curves were obtained by fitting DFT-LDA-CPM band-gap calculations to $\Delta E_g = \beta d^{-\alpha}$ (see text). The threshold diameters (d_{th} values) were determined to be 72.1 nm (not shown) and 15.4 nm (gray line) when the Coulomb energies in the dots were omitted and included, respectively.

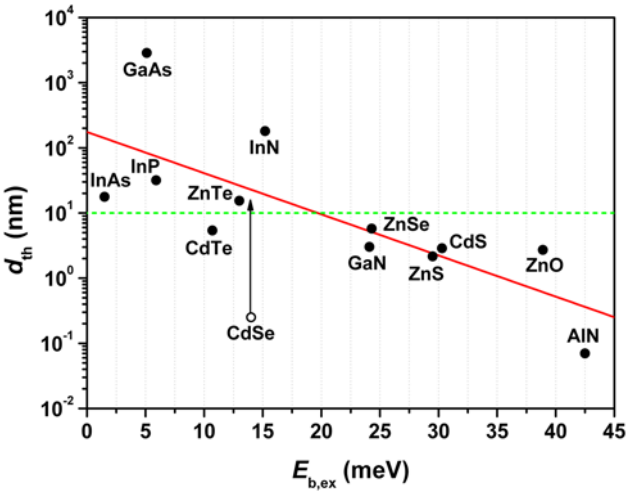

Figure 7. Log-normal plot of threshold diameter vs. calculated bulk exciton binding energy for various II-VI and III-V semiconductors. The red line is the linear least-squares fit to the solid data points. The green dashed line shows a threshold diameter of 10 nm; systems having threshold diameters below this value will exhibit dot and wire band-gap energies that are not currently experimentally distinguishable (see text). Consequently, with the exception of CdSe (see text), we should not be able to measure EMA-PIB A_{wire}:A_{dot} slope ratios (approaching 0.6) for semiconductor systems that fall below the green dashed line. The arrow indicates what we believe to be the actual placement of the CdSe point.

Table of Contents (TOC) Graphic

Synthesis of Cadmium Telluride Quantum Wires and the Similarity of Their Band Gaps to Those of Equidiameter Cadmium Telluride Quantum Dots

Jianwei Sun, Lin-Wang Wang, and William E. Buhro